Multimodal integration of high-resolution EEG and functional magnetic resonance imaging data: a simulation study

F. Babiloni,[a,*] C. Babiloni,[a,c] F. Carducci,[b,d] G.L. Romani,[b,e] P.M. Rossini,[c,d,f]
L.M. Angelone,[a] and F. Cincotti[a,g]

[a] *Dipartimento di Fisiologia Umana e Farmacologia, Università di Rome "La Sapienza," Rome, Italy*
[b] *Dipartimento di Scienze Cliniche e Bioimmagini and Istituto di Tecnologie Avanzate Biomediche, Università "G. D'Annunzio," Chieti, Italy*
[c] *IRCCS "San Giovanni di Dio" Istituto Sacro Cuore di Gesù, Brescia, Italy*
[d] *AFaR and CRCCS Ospedale Fatebenefratelli, Isola Tiberina, Rome, Italy*
[e] *Istituto Nazionale di Fisica della Materia, UdR, L'Aquila, Italy*
[f] *Cattedra di Neurologia, Università Campus Bio-Medico, Rome, Italy*
[g] *IRCCS Fondazione "Santa Lucia," Rome, Italy*

Abstract

Previous simulation studies have stressed the importance of the use of fMRI priors in the estimation of cortical current density. However, no systematic variations of signal-to-noise ratio (SNR) and number of electrodes were explicitly taken into account in the estimation process. In this simulation study we considered the utility of including information as estimated from fMRI. This was done by using as the dependent variable both the correlation coefficient and the relative error between the imposed and the estimated waveforms at the level of cortical region of interests (ROI). A realistic head and cortical surface model was used. Factors used in the simulations were the different values of SNR of the scalp-generated data, the different inverse operators used to estimated the cortical source activity, the strengths of the fMRI priors in the fMRI-based inverse operators, and the number of scalp electrodes used in the analysis. Analysis of variance results suggested that all the considered factors significantly afflict the correlation and the relative error between the estimated and the simulated cortical activity. For the ROIs analyzed with simulated fMRI hot spots, it was observed that the best estimation of cortical source currents was performed with the inverse operators that used fMRI information. When the ROIs analyzed do not present fMRI hot spots, both standard (i.e., minimum norm) and fMRI-based inverse operators returned statistically equivalent correlation and relative error values.
© 2003 Elsevier Science (USA). All rights reserved.

Keywords: Linear inverse source estimate; EEG and fMRI integration; Movement-related potentials

Introduction

Electroencephalography (EEG) is a useful technique for the study of brain dynamics and functional cortical connectivity, because of its high temporal resolution (milliseconds; Nunez, 1995, 1981). EEG reflects the activity of cortical generators oriented both tangentially and radially with respect to the scalp surface. However, the different electrical conductivity of brain, skull, and scalp markedly blurs the EEG potential distributions and makes the localization of the underlying cortical generators problematic. Neural sources of EEG can be localized by making on a priori hypothesis on their number and extension. When the EEG activity is mainly generated by a known number of cortical sources (i.e., short-latency evoked potentials), the location and strength of these sources can be reliably estimated by the dipole localization technique (Scherg et al., 1984). However, with the exception of the early processing of sensory responses, event-related cortical responses include a distributed network of several and unknown areas. When the distributed cortical network is supposed to be active, corti-

---

* Corresponding author. Dipartimento di Fisiologia Umana e Farmacologia, Università di Roma "La Sapienza," P.le A. Moro 5, 00185 Rome, Italy. Fax: +39-06-49910917
E-mail address: Fabio.Babiloni@uniromal.it (F. Babiloni).

cal sources of EEG data should be modeled by linear inverse estimation (Dale and Sereno, 1993; Dale et al., 2000). This approach implies the use both of thousands of equivalent current dipoles as a source model and of realistic head models, reconstructed from magnetic resonance images, as a volume conductor medium. The use of geometrical constants can generally reduce the solution space (i.e., the set of all possible combinations of the cortical dipoles strengths). For example, the dipoles can be disposed along the reconstruction of cortical surface with a direction perpendicular to the local surface. An additional constraint is to force the dipoles to explain the recorded data with a minimum or a low amount of energy (minimum-norm solutions; Dale and Sereno, 1993; Hämäläinen and Ilmoniemi, 1984). The solution space can be further reduced by using information deriving from hemodynamic measures (i.e., functional magnetic resonance imaging (fMRI)–BOLD phenomenon) recorded during the same task. The rationale of a multimodal approach is that neural activity, modulating neuronal firing and generating EEG potentials, increases glucose and oxygen demands (Magistretti et al., 1999; Liu et al., 1998; Dale et al. 2000). This results in an increase in the local hemodynamic response that can be measured by fMRI (Grinvald et al., 1986; Puce et al., 1997). Hence, fMRI responses and cortical sources of EEG data can be spatially related (Logothetis et al., 2001).

Determination of the priors in the resolution of the linear inverse problem was performed with the use of information from the hemodynamic responses of the cortical areas (Liu et al., 1998; Dale et al., 2000). In using the block-design fMRI priors for the estimation of current strengths we failed to take into account information about the coupling of the neural sources. Previous approaches of the cortical current density estimation used only the diagonal elements of the matrix that describes the prior estimates of the dipole strength variance as a function of the corresponding fMRI activation (Liu et al., 1998; Liu 2000). However, it is also possible to insert the information of the coupling of the hemodynamic activity between different cortical sources by means of the off-diagonal terms of such matrix (Liu, 2000; Cincotti et al., 2001; Babiloni et al., 2002). Technically, this information was coded through the off-diagonal elements of the source metric of the inverse problem, while the diagonal elements of this metric were equal to those already used by the standard fMRI-based inverse operators. To estimate the hemodynamic correlation of the neural sources, we used the hemodynamic responses of the event-related fMRI and the time course of the source responses. This estimate was evaluated computing the cross-correlation on the hemodynamic waveforms obtained by the averaged fMRI activity in the analyzed region of interest. Namely, the amount of information stored for the solution of the inverse problem by using also the off-diagonal terms of the source-metric matrix is superior to those encoded by using the standard fMRI-based inverse operators (Liu, 2000). However, it still must be proved, through appropriate simulations whether this increased amount of information could be useful for the estimation of cortical current density.

Previous simulation studies (Liu et al., 1998; Liu, 2000) have focused on the efficacy of the estimation of cortical current density by using fMRI priors under a particular level of the signal-to-noise ratio (SNR;10) and a particular number of MEG sensors (122). On the other hand, commonly encountered event-related potentials/fields showed values of SNR equal to 5, 3, or even 1 (Regan, 1989). Either 29 or 61 electrodes, placed on the scalp in agreement with the standard of the extension of the old International 10/20 system (Regan, 1989), are also commonly used in the EEG literature. For these reasons, we would like to investigate the effects of the inclusion of different kinds of fMRI priors for the estimation of the cortical current density under different numbers of sensors and different levels of SNR of the used data. Simulations were performed with the aid of realistic head volume-conductor model and a realistic cortical surface, derived from magnetic resonance imaging of an experimental subject. On the cortical reconstruction we considered seven region of interest (ROI), in which simulated cortical waveforms were generated. The estimation process retrieved the cortical waveforms at the ROI level. First, the estimation of current density for each one of the 3000 current dipoles used was performed. Second, the average of cortical waveforms within each particular ROI considered was computed. The dependent variables used for the statistical analysis were the relative errors and the correlation coefficient values between the estimated and the generated waveforms at the cortical level in each ROI analyzed.

The specific questions at the base of the present experimental design are:

1. What is the influence of the variable SNRs and the number of electrodes used on the estimation of the cortical current density by using (or not) fMRI priors?
2. Does the use of fMRI priors increase the efficacy of the cortical current density estimation in the ROIs in which fMRI hotspots are present?
3. Does the use of fMRI priors decrease the efficacy of the cortical current density estimation in the ROIs in which there are no fMRI hotspots?

Methods

Head and cortical models

For the stimulation purposes, we used a subject's realistic head model reconstructed from TI-weighted MRIs (256 images; 256 × 256 pixels; voxel size 1.0 × 1.0 × 1.0). Scalp, skull, and dura mater compartments were segmented from MRIs and triangulated with about 1000 triangles for each surface. Sources model was built with the following procedure: the cortex compartment was segmented from MRIs and triangulated obtaining a fine mesh with about

100,000 triangles; a coarser mesh was obtained by resampling the fine mesh previously described to about 3000 triangles (this was done by preserving the general features of the neocortical envelope, especially in correspondence of pre- and postcentral gyri and frontal mesial area); and an orthogonal unitary equivalent current dipole was placed in each node of the triangulated surface, with direction parallel to the vector sum of the normals to the surrounding triangles.

Estimation of cortical source current density

The solution of the following linear system:

$$\mathbf{A}\mathbf{x} = \mathbf{b} + \mathbf{n} \tag{1}$$

provides an estimation of the dipole source configuration **x** that generated the measured EEG potential distribution **b**. The system includes also the measurement noise *n,* supposed normally distributed.

Also, in Eq. (1) **A** is the lead field matrix, in which each *j*th column describes the potential distribution generated on the scalp electrodes by the *j*th unitary dipole. In the EEG case the electrical lead field matrix **A** and the data vector **b** must be referenced consistently. Among the several equivalent solutions for the underdetermined system (1), the current density solution vector ξ was chosen by solving the following variational problem for the sources **x** (Grave de Peralta and Gonzalez Andino, 1998):

$$\xi = \arg\min \left(\|\mathbf{A}x - b\|_{\mathbf{M}}^2 + \lambda^2 \|x\|_{\mathbf{N}}^2 \right), \tag{2}$$

where **M** and **N** are the matrices associated with the metrics of the data and of the source space, respectively, λ is the regularization parameter, and $x_{\mathbf{M}}$ represents the **M** norm of the vector **x**. The solution of the variational problem depends on the adequacy of the data and source space metrics. Under the hypothesis of **M** and **N** positive definite, the solution of Eq. (2) is given by computing the pseudoinverse matrix **G** (often called inverse operator) according to the following expressions:

$$\xi = \mathbf{G}b, \quad \mathbf{G} = \mathbf{N}^{-1}\mathbf{A}' \left(\mathbf{A}\mathbf{N}^{-1}\mathbf{A}' + \lambda\mathbf{M}^{-1} \right)^{-1} \tag{3}$$

An optimal regularization of this linear system was obtained by the L-curve approach (Hansen, 1992a). This curve, which plots the residual norm versus the solution norm at different λ values, was used to choose the optimal amount of regularization in the solution of the linear inverse problem. Computation of the L-curves and optimal λ correction values was performed with the original routines of (Hansen 1992b). The metric **M** characterizes the idea of the closeness in the data space. It can be particularized taking into account the sensors noise level, using either the Mahalanobis distance (Grave de Peralta and Gonzalez Andino, 1998) or the identity matrix (Hämäläinen and Ilmoniemi, 1984). On the other side, the source metric **N,** as shown in the next section, can be particularized by means of the a

priori information of the hemodynamic responses of the single voxels, as derived from the fMRIs.

Electrical source constraints

For the solution of the linear inverse problem two characterizations of the inverse source metric **N** are very popular in literature. The first one is the so-called minimum-norm source metric (Hämäläinen and Ilmoniemi, 1984), in which no a priori information on the sources is available. In this case, the inverse of the source metric is represented by the equation

$$\mathbf{N}^{-1} = \mathbf{I}, \tag{4}$$

where **I** is the identity matrix and $\mathbf{N}^{-1}$ is the inverse of the source metric matrix.

The second characterization of the source metric **N** takes into account all the cortical voxels on the basis of their electrical "closeness" to the EEG sensors. This allows us to remove the voxels inverse dependence on the sensor-to-dipole distance (column norm normalization; Pascual-Marqui, 1995). In this case, the inverse of the resulting source metric **N** is

$$(\mathbf{N}^{-1})_{ii} = \|\mathbf{A}_{\cdot i}\|^{-2}, \tag{5}$$

where $(\mathbf{N}^{-1})_{ii}$ is the ith element of the inverse of the diagonal matrix **N** and all the other matrix elements $\mathbf{N}_{ii}$ are set to 0. The L2 norm of the *i*th column of the lead field matrix **A** is denoted by $\|\mathbf{A}_{\cdot i}\|$. The inverse operators characterized by the choice of the source metric described by Eqs. (4) and (5) are referred in this paper as minimum norm (MN) and column-normalized minimum norm (MNC), respectively.

Functional hemodynamic coupling constraints

The information related to the statistical hemodynamic activation of *i*th cortical voxels can be included into the linear inverse estimation. We will now present two different ways in which this can be implemented.

The introduction of fMRI priors into the linear inverse estimation produces a bias in the estimated solution vector. Statistically significantly activated fMRI voxels, returned for instance by the so-called percentage change approach (Kim et al., 1993), are taken into account as weights for the EEG-measured potentials. The inverse of the resulting source metric **N** is now

$$(\mathbf{N}^{-1})_{ii} = g(\alpha)^2 \tag{6}$$

$$(\mathbf{N}^{-1})_{ii} = g(\alpha)^2 \|\mathbf{A}_{\cdot i}\|^{-2}, \tag{7}$$

where $(\mathbf{N}^{-1})_{ii}$ and $\|\mathbf{A}_{\cdot i}\|$ have the same meaning described above for the *i*th cortical voxel examined. The $g(\alpha_i)$ is a function of the statistically significant percentage increase of the fMRI signal during the task, compared to the rest state. This function $g(\alpha_i)$ is assigned to the *i*th dipole of the

modeled source space. A possible way to express such function is.

$$g(\alpha_i)^2 = 1 + (K - 1)(\alpha_i/\max(\alpha_i)),$$

$$K \geq 1, \; \alpha_i \geq 0, \quad (8)$$

where α_i is the statistically significant percentage increase of the fMRI signal during the task state for the ith voxel. It must be noted that different choices of $g(\alpha_i)$ function are possible for the ith cortical voxel examined. For instance, setting $g(\alpha_i) \propto \alpha_i$ only if α_i is statistically significantly increased compared to the rest state, and zero elsewhere (George et al., 1995). Another possible way to set the $g(\alpha_i)$ function is $g(\alpha_i) = \Lambda$, (with $\Lambda \in [0 \; 1]$), for each ith brain voxel in which the α_i is statistically significantly increased during the task with respect to the rest state and 1 elsewhere (a typical choice is $\Lambda = 0.1$; Liu et al., 1998; Liu, 2000). In Eq. (8), the value of the parameter K tunes the strength of the inclusion of the fMRI constraints in the source space. Setting $K = 1$ let us disregard fMRI priors, thus returning to a purely electrical solution (equals to the MN and MNC inverse operators). Instead, a value of $K \gg 1$ allows only the sources associated with fMRI active voxels to participate in the solution of the linear inverse problem. The inverse operators for the estimation of the cortical activity obtained with the use of the source metric expressed by Eqs. (6) and (7) will be denoted in the following as diag-fMRI and diag-fMRINC, respectively.

Both the previous definitions of the source metric **N** (Eqs. (6) and (7) result in a matrix with the off-diagonal elements equal to zero. Now, using the off-diagonal elements of the matrix **N** we are able to insert the information about the functional hemodynamic coupling of the cortical sources. In particular, we set the generic ij entry of the inverse of matrix **N** as

$$(\mathbf{N}^{-1})_{ij} = g(\alpha_i) \, g(\alpha_j) \cdot \mathrm{corr}_{ij} \qquad (9)$$

$$(\mathbf{N}^{-1})_{ij} = g(\alpha_i) \, g(\alpha_j) \|\mathbf{A}_{.i}\|^{-1} \|\mathbf{A}_{.j}\|^{-1} \cdot \mathrm{corr}_{ij}, \qquad (10)$$

where $\|\mathbf{A}_{.i}\|$ and $g(\alpha_i)$ have the same meaning described above for the ith cortical voxel examined. corr_{ij} is the degree of functional coupling between the ith source and the jth source j during the particular task analyzed, as revealed by computing the correlation of their hemodynamic responses from the event-related fMRI data. The inverse operators obtained with the use of the source metric presented in Eqs. (9) and (10) will be denoted as corr-fMRI and corr-fMRINC, respectively. It is worth noticing that in the case of uncorrelated sources ($\mathrm{corr}_{ij} = 0$, $i \neq j$; $\mathrm{corr}_{ii} = 1$), the corr-fMRI formulation leads back to the diag-fMRI one.

Regions of interest and electrode arrays

Seven cortical ROIs were drawn by two independent and expert neuroradiologists on the computer-based cortical reconstruction of the head model used for simulations. These ROIs were those related to the primary right and left sensorimotor (S1 and M1) and to the supplementary motor area (SMA). In particular, the ROIs representing the left and right S1 areas included Brodmann areas (BA) 3, 2, 1, while the ROIs representing the left and right M1 included BA 4. The ROIs representing the SMA region were obtained from the cortical voxels belonging to BA 6. There were no attempts to separate the proper and anterior SMA. Furthermore, ROIs from the right and the left posterior parietal areas (denoted in the following as PP; including at large the BA 5, 7, 39, 40, 43) were considered. These last two cortical regions were used to model cortical areas that are larger than conventional BA used for the other ROIs.

Three electrodes arrays were considered. The first one had 128 electrodes regularly disposed on the scalp surface. The others had 61 and 29 electrodes, resulted from a regular downsampling of the full electrode configuration. This subsampling aimed to simulate both standard (29) and high-resolution EEG recordings (61 and 128), in agreement with the standard of the extension of the International 10/20 system (Sharbrough et al., 1991). Fig. 1 shows the different electrode arrays used in the simulation on the realistic head model and the ROIs used in the simulation process.

Source reference waveforms

Seven source waveforms estimated from a high-resolution movement-Related potentials (MRP) recording (128 electrodes) were used as reference for the simulation. The EEG was recorded in a healthy subject who executed a set of unaimed, self-paced, and brisk movements of the right middle finger. The original MRP data were sampled at 300 Hz, from 3S before to 2 after the EMG onset (1500 data points). To reduce the dimension of the data set, this was downsampled to 128 data points after proper low-pass, finite impulse response and zero phase filtering. The collapsed source waveforms were estimated by means of the minimum-norm inverse operator (Hämäläinen and Ilmoniemi, 1984; Dale and Sereno, 1993), with the head volume conductor, cortical models, and the ROIs described above (thus the same used for the simulations)

Distribution of fMRI activated dipoles along the ROIs

Three of the seven ROIs considered in this study were chosen as site for the fMRI activations: specifically, the ROIs modeling the left S1, the left M1, and the SMA. In the cortical regions with fMRI hot spots, in different simulations different percentages of coverage of the cortical ROI voxels were used (25, 50, and 100%). Moreover, for each simulation, the same percentage of coverage was used for all the ROIs with fMRI hot spots. Each jth value of the inverse of the source metric (N) of a jth dipole belonging to a particular ROI was associated with a prefixed $g(\alpha_j)$ value,

according to Eq. (7) or Eq. (10). These values were estimated from standard fMRI recordings at 1.5 T, performed on the same experimental subject used for EEG recordings. Block-design and event-related fMRI acquisitions during the same voluntary right-middle finger extensions were performed. Max values of α at 1.2% were found in the analyzed movement task using the statistically significant brain voxels detected by MEDEX software.

Using the event-related fMRI data acquired, we computed the average correlation coefficient between the hemodynamic waveforms of each voxel that belongs to a ROIs similar to those used in the simulation study (primary somatosensory and motor area, supplementary motor area). This average value of correlation ($corr_{ij} = 0.85$) was hence used to characterize the off-diagonal terms described in Eqs. (9) and (10) for all the current dipoles belonging to the same ROI. Also, from the event-related fMRI recording we estimated the average correlation values between the hemodynamic waveforms of brain voxels belonging to the different ROIs. We used this average value ($corr_{Zij} = 0.7$) in Eqs. (9) and (10) for all the off-diagonal terms of the fMRI inverse operator related to current dipoles belonging to different ROIs.

The dependent variables used

In the different experimental conditions, the accuracy of the estimated cortical current strengths array (**Es**) from the generated one (**Gs**) was evaluated by computing two indexes, to be used in the simulations as dependent variables. The first one was the correlation coefficient (CC) between the generated and the estimated average source waveforms, according to the formula

$$CC = \frac{Gs \bullet Es}{\sqrt{\|Gs\|_2^2 \cdot \|Es\|_2^2}}, \tag{11}$$

where $\bullet$ stands for the usual inner products between the **Gs** and the **Es** vectors. The second one was the relative error (RE), computed according to the formula

$$RE = \frac{\|Gs - Es\|_2}{\|Gs\|_2}, \tag{12}$$

where $\|\mathbf{x}\|_2$ is the standard L2 norm of a vector $\mathbf{x}$.

Experimental design

The experimental design, also represented in Fig. 2, was drawn as follows:

1. By means of the electric lead field matrix the source reference waveforms were propagated, through the realistic volume conductor, in the direction of the simulated electric sensor arrays. The arrays had variable numbers of electrodes (128, 61, 29). Depending on this numbers, three separate HREEG data sets were produced.
2. Variable coverage of fMRI hot spots of left S1, left M1, and SMA areas was performed at three different percentages (25, 50, and 100%) (point 2 of Fig. 2).
3. White noise was added to these three data sets, to reach seven different levels of signal-to-noise ratios (SNRs; infinite, 30, 20, 10, 5, 3, 1). This recalls the typical range of SNR commonly encountered in evoked, motor-related, and cognitive-related EEG recordings, respectively (points 3 and 4 of Fig. 2).
4. The inverse electric operators described above were applied to these EEG data sets and the consequent cortical activity was estimated in each ROI. Six types of weights for the inverse operators have been used: the minimum norm estimate (MN, Eq. (4)), the column normalized minimum norm estimate (MNC, Eq. (5)), the block-design fMRI constraint both with and without the column normalization (diag-fMRI and diag-fMRI NC, Eqs. (6) and (7), respectively), and the event-related fMRI constraint both with and without column normalization (corr-fMRI and corr-fMRI NC, Eqs. (9) and (10), respectively) (point 5 of Fig. 2).
5. For each ROI the estimated current source density was the average of the current estimates of all the dipoles belonging to the ROI (point 6 of Fig. 2).
6. The adequacy of the reconstructed cortical activity was analyzed by computing the CC and the RE at ROI level between the generated and the estimated activities, along all the simulated trials.

For each level of SNR adopted, 32 occurrences of white noise data were considered on the simulated EEG scalp waveforms. This resulted in 32 values of CC and RE variables for each level of the independent variables considered. These computations were performed to increase the reliability of the statistical results obtained. The average values of

---

Fig. 1. The head model with the region of interests (ROI) used in this study. The ROIs representing the supplementary motor area, the primary somatosensory area and the motor area. (Top row) Different electrode arrays used in this simulation study. Right, full array with 128 electrodes; center, array with 61 electrodes; and left, downsampling at 29 electrodes.

Fig. 2. Different steps involved in this simulation study. (1) Generation of the signal at the cortical level; (2) fMRI hot spots coverage of the ROI at 25, 50, and 100%; (3) generation of the EEG signal by means of the realistic head model and the different EEG electrodes arrays (29, 61, and 128 electrodes); (4) simulated EEG signal plus white noise at different levels of SNR (infinite, 30, 20, 10, 5, 3, 1); (5 and 6) estimation of current density at the ROI level with the different inverse operators; (7) comparisons between the estimated and the generated cortical waveforms by means of correlation coefficient (CC) and relative error (RE) indexes.

1

2

In the figure: $n_i(t)$, $b_i(t)$, $+$

③

④ Simulated EEG

⑤ Inverse operator

⑥

Estimated signal

① Generated signal

② fMRI hotspots coverage

⑦ CC, RE
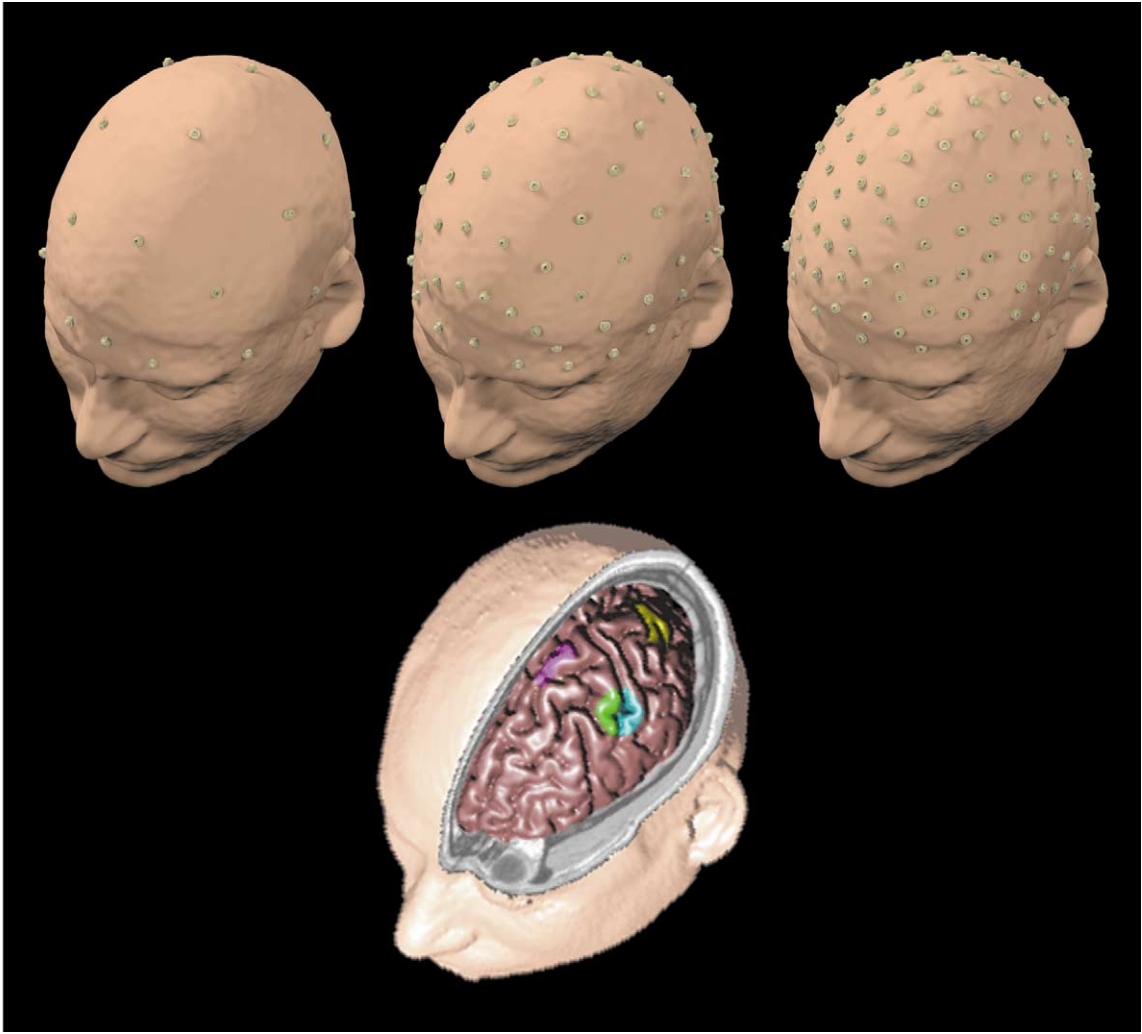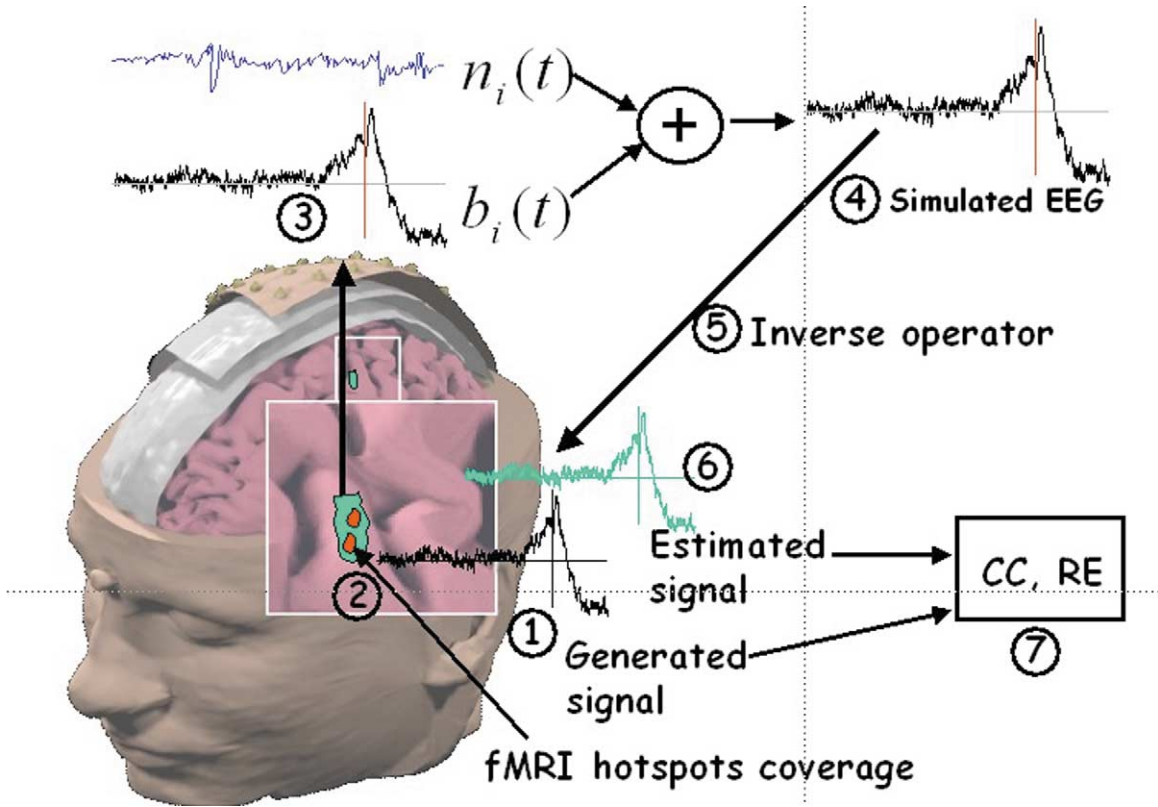
3
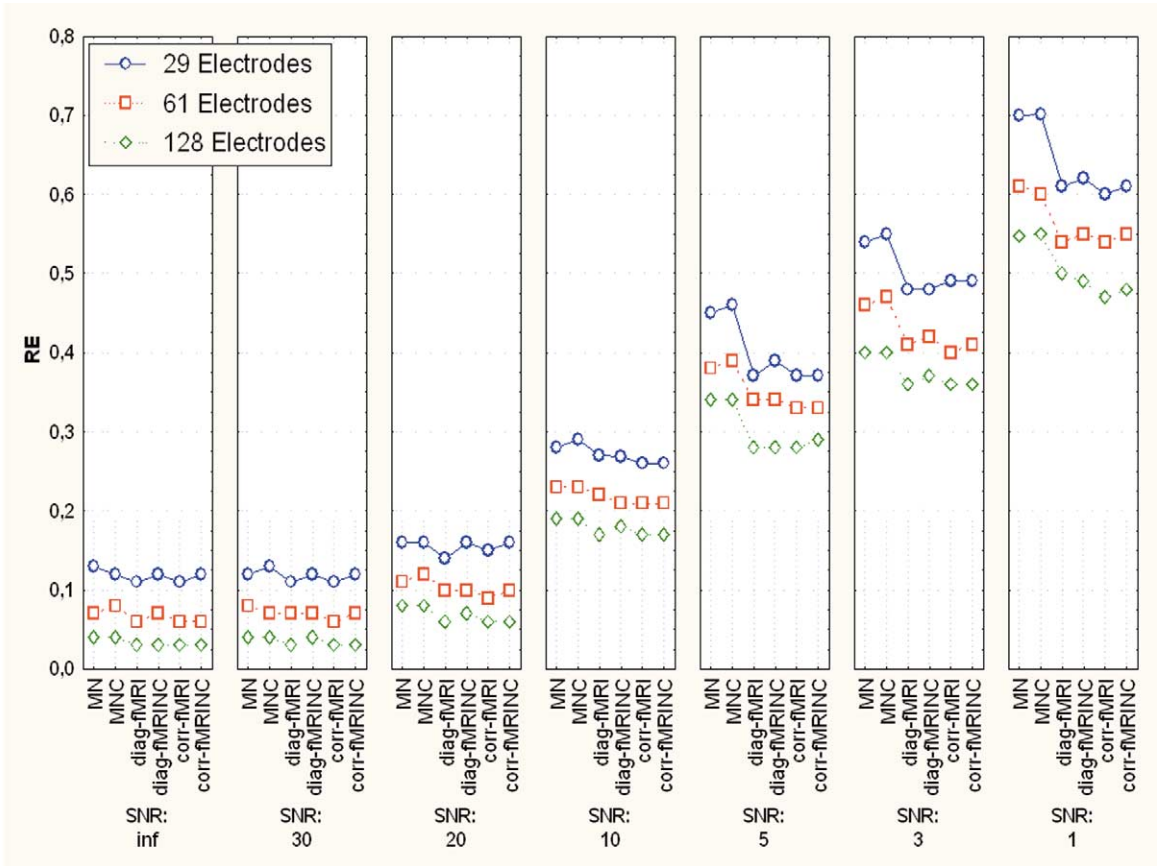
4
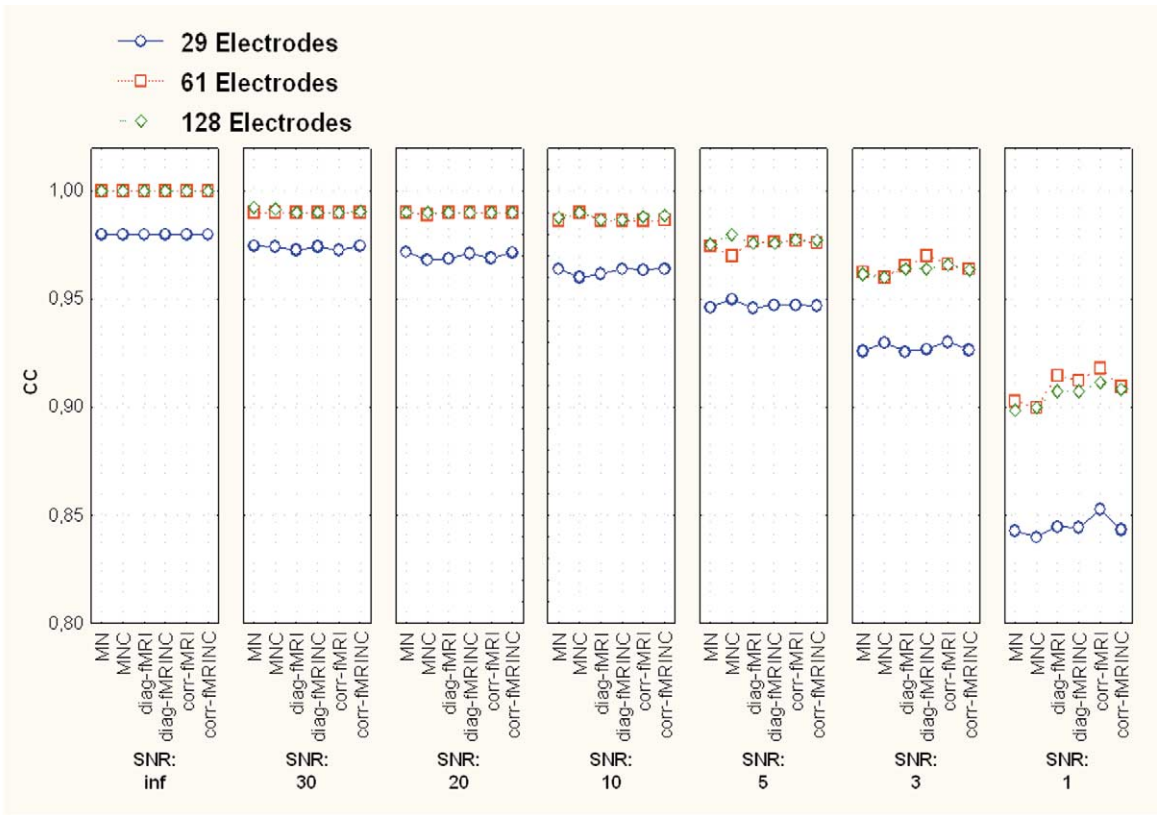
Table 1
Independent variables used for the statistical analysis of the estimated current densities and their relative levels of variation

Variable	Description	Levels
FMRISTRENGTH	Values of the K factor in the fMRI-based inverse operators	3, 5, 7, 10
FMRICOVERAGE	Percentage of the ROI covered by fMRI hot spots	25, 50, 100
SNR	Signal-to-noise ratio generated at the EEG sensors	∞, 30, 20, 10, 5, 3, 1
INVERSE	Type of inverse operator, described by Eqs. (4)–(10)	MN, MNC, diag-fMRI, diag-fMRINC, corr-fMRI, corr-fMRINC
ELECTRODES	Number of simulated scalp electrodes	29, 61, 128

CC and RE were then used in the successive statistical analysis.

Statistical analysis

The obtained results were subjected to separate analysis of variance (ANOVA). The main factors of the ANOVAs were the SNR (with seven levels: infinite, 30, 20, 10, 5, 3, 1), the type of inverse operator used (with and without fMRI constraints, with six levels) denoted as INVERSE; the value of K parameter for the fMRI-based inverse operator (with four levels: 3, 5, 7, and 10), denoted as fMRISTRENGTH; and the number of electrodes of the recording array (ELECTRODES, with three levels: 128, 61, and 29). Separate ANOVAs were performed on CC and RE data obtained for the full array of 128 electrodes to understand the effect of the number of fMRI hot spots for each analyzed ROI (fMRICOVERAGE, with three levels: 25, 50, and 100%). Table 1 reports the independent variables and their relative levels of variations used.

In all the evaluated ANOVAs, the correction of Greenhouse–Gasser for the violation of the spherical hypothesis was used. The post hoc analysis with the Scheffe's test at the $P = 0.05$ statistical significance level was then performed.

Results

Effects of the intensity of fMRI priors on the current density estimation

For each ROI the analysis of the simulation results was performed separately. All the performed ANOVAs included the following main factors: fMRISTRENGTH, SNR, and INVERSE. Simulations were performed using data from the 128 electrodes and fMRI coverage of 100% of left S1, left M1, and SMA ROIs. Both CC and RE indexes were used.

All the seven ANOVAs performed (one for each ROI analyzed) returned a coherent and similar pattern of results depending or not on the inclusion of fMRI hot spots in the ROI analyzed. In the following we present data for the SMA as representative of the ROIs with fMRI hot spots included and data from the right PP as representative of the ROIs without fMRI hot spots included. This can be done without loss of generality.

ROI with the presence of fMRI hotspots

For all the main factors analyzed and their interactions with $P < 0.0001$, the three-way ANOVA returned statistically significant values for both CC and RE indexes, evaluated on the ROI representing the SMA. Similar results to those obtained for the ROI representing the SMA were found in all the other ROIs with the fMRI hot spots included, that is, the left primary somatosensory and left motor area. In particular, the results were only different in the absolute values of the F scores. Also, for the left S1 and the left M1 all the main factors investigated as well as all their interactions resulted statistically significant with $P < 0.001$. The analysis of the post hoc tests performed for all the ROIs covered with fMRI hot spots revealed that fMRI-based inverse operators (diag-fMRI, diag-fMRINC, corr-fMRI, corr-fMRINC) reached statistically significant higher values of CC with respect to the inverse operators that do not use fMRI constraints (MN and MNC). Among the fMRI-based inverse operators, the value of fMRISTRENGTH of $K = 3$ returned the best CC results for a large set of SNR levels when compared with all the others ($K =$

Fig. 3. Seven panels are shown, one for each particular value of SNR used in simulations. In each panel the vertical axes reports the average of the relative error (RE) index computed after the current density estimation. Also, the horizontal axis reports the different inverse operators used for the estimation of current density. Each data point represents an averaged value of the RE index, corresponding to a particular SNR and a particular inverse operator in the simulations performed. Three different symbols are used to characterize the estimation performed with data from 29 electrodes (circles), 61 electrodes (squares), and 128 electrodes (diamonds). Significant reductions of RE values were noted for the fMRI-based inverse operators with respect to the other inverse methods with SNR values between 5 and 1. Simulations performed with an fMRI hot spots percentage coverage of the ROI equal to 100%, and a level of fMRI strength equal to 3.

Fig. 4. Average data for correlation coefficient (CC) in the right posterior parietal (PP) ROI at the different levels of the main factors considered (ELECTRODES, INVERSE, and SNR). Simulations performed at 100% of fMRI coverage for the ROIs SMA, left S1, and left M1. Same conventions used for Fig. 3. Simulations performed with an fMRI hot spots percentage coverage of the ROI equal to 100%, and a level of fMRI strength equal to 3. Same conventions are used for Fig. 3.

5, 7, and 10) with the post hoc tests. This holds true in all the post hoc comparisons in which the SNR moves from infinite to 5 at a statistical significance level of $P < 0.001$. Comparisons at low SNR values (3 and 1) returned less but still statistical significant differences in CC ($P < 0.01$) between the estimation obtained for $K = 3$ and the other conditions analyzed ($K = 5, 7$, and 10).

The simulations illustrated above were also evaluated by computing the RE index. The results of the ANOVA showed that all the main factors and their interaction were significant at $P < 0.0001$. In this case there were also statistical significant interactions of the main factors used in the ANOVA. For all the ROIs analyzed, at different SNR levels, the values of the RE obtained with the fMRI-based inverse operators (diag-fMRI and corr-fMRI) were statistically significant lower compared to the minimum-norm and weighted-minimum-norm inverse operators. However, for all the inverse methods and the different conditions of SNR used in the simulations, the Scheffe's post hoc tests reported no significant statistical differences between the lower RE values obtained with either $K = 3$ or $K = 10$ as fMRI strengths. For both levels of fMRI strengths ($K = 3$ and $K = 10$) we obtained RE values that are statistically significantly lower than those obtained with other K values ($P < 0.001$). Hence, in the following the fMRI strength of $K = 3$ will be used for both CC and RE variables with variable number of electrodes, inverse operators, and SNR levels. The post hoc tests between RE and CC indexes obtained by using diag-fMRI- and corr-fMRI-based inverse operators reported no significant differences under almost the totality of the SNRs used. The post hoc tests were generated between the fMRI-based inverse operators that used the same fMRISTRENGTH factor ($K = 3$ or $K = 10$) chosen on the basis of previous analysis. Furthermore, no differences were observed between the depth-weighted fMRI-based inverse operators (diag-fMRINC, corr-fMRINC) and their unweighted counterpart (diag-fMRI, corr-fMRI) under the same range of SNRs analyzed. The only differences in accuracy, for the estimation of cortical current density between the inverse operators, were present for the RE index in the condition of SNR = 1. In this case, the corr-fMRI inverse operator performs current estimations characterized by lower values of RE index compared to the other fMRI-based methods (at a significance level of $P < 0.01$). These lower values of RE were observed for both the best K values used (3 and 10). The effects described for the fMRI-based inverse operators hold in all the ROIs characterized with the presence of fMRI hot spots.

ROI without the presence of fMRI hotspots

The results obtained for the ROIs without the fMRI hot spots, namely the right M1, the right S1, and the left and right PP area, showed a statistical equivalence of the CC and RE indexes with respect to the different levels of the main factors fMRISTRENGTH and INVERSE. The fMRI-STRENGTH factor was investigated for this type of ROI

without fMRI priors, while the current density estimation was simultaneously performed also for the other ROIs with fMRI priors. The main factor SNR was instead significant in reducing the variance of CC and RE data. We reported the statistical results for the ROI right PP, as example for the other ROIs without fMRI hot spots that were analyzed. More specifically, no significant reduction in variances of CC index occurred when the main factors fMRI-STRENGTH ($F(3,93) = 1.84$; $P < 0.14$) and INVERSE ($F(5,155) = 1.64$; $P < 0.15$) were considered. The main factor SNR was instead useful to reduce the data variance ($F(6,186) = 2.22$; $P < 0.05$). No significant interactions between the main factors were found. The RE index returned for the right PP ROI a similar picture of that obtained with the analysis of CC index. In fact, no statistical significant reduction of RE data variance for the main factors fMRISTRENGTH ($F(3,93) = 1.44$; $P < 0.23$) and INVERSE ($F(5,155) = 1.95$; $P < 0.09$) was observed, while the main factor SNR was instead found significant ($F(6,186) = 2.3$; $P < 0.036$). No other statistically significant interactions between the main factors were found for the ROIs without the presence of fMRI hot spots.

Effects of inverse methods, number of electrodes, and SNR levels on the cortical current density estimation

Evaluation at constant fMRI hot spot percentage coverage (100%) and at constant level of strength of the fMRI priors

The following explains an analysis of the accuracy of the estimation of cortical current density as obtained by using a constant fMRI hot spots percentage coverage of the SMA, left S1, and left M1 (equal to 100%) and a constant level of fMRI strength (equal to $K = 3$) for the fMRI-based inverse operators. As in the previous case, separate analyses were performed for each ROI. All the performed ANOVAs included the main factors ELECTRODES (with three levels: 29, 61, and 128), INVERSE (six levels: MN, MNC, diag-MN, diag-MNC, corr-MN, corr-MNC), and SNR (with seven levels: infinite, 30, 20, 10, 5, 3, and 1).

ROIs with presence of fMRI hot spots

Because of the similarity of the statistical results obtained in each one of the ROIs that have fMRI hot spots (left S1, left M1, and SMA), only the results for the ROI corresponding to the SMA are reported. A three-way ANOVA was performed for both CC and RE as dependent variables, including the main factors ELECTRODES, INVERSE, and SNR. All the main factors used as well as their interactions reduced the variance of CC and RE indexes in a statistical significant way (all tests returned significant levels of $P < 0.0001$).

Regarding to the CC index, the inverse operators that used fMRI priors for the estimation of cortical current densities significantly improved the reconstruction of the cortical activity with respect to the standard inverse opera-
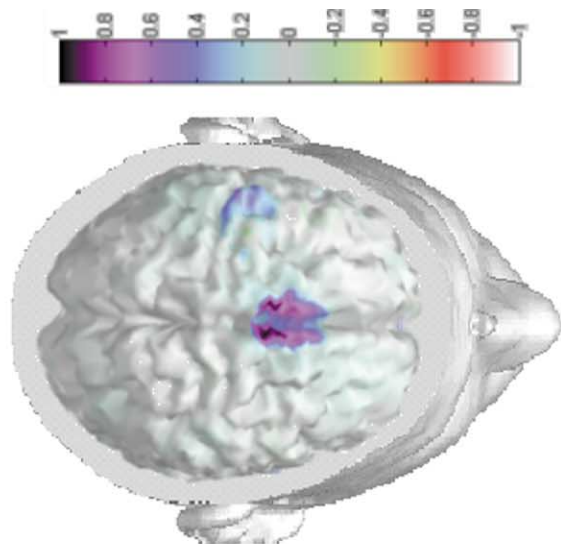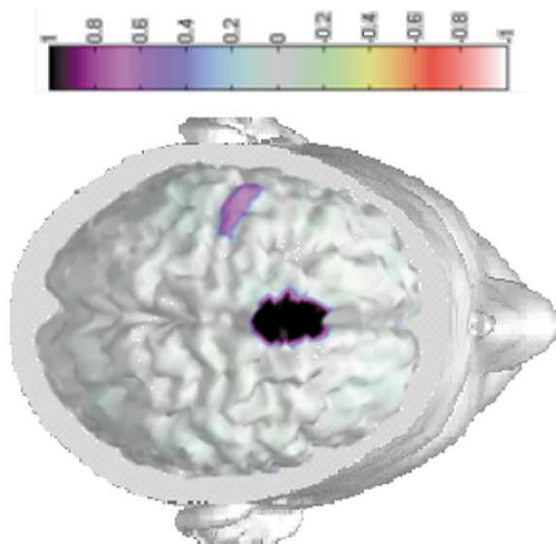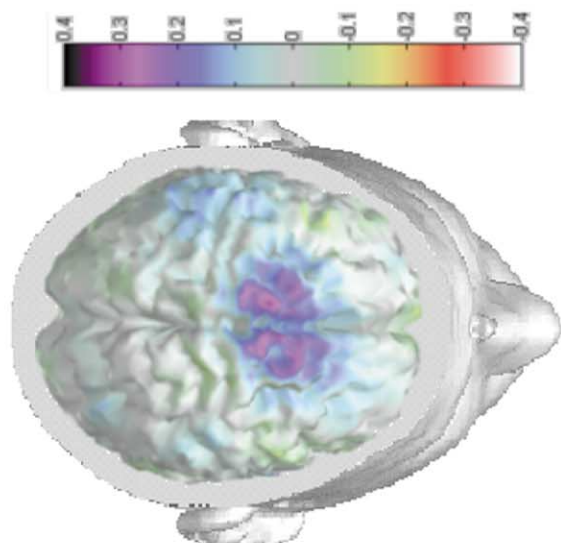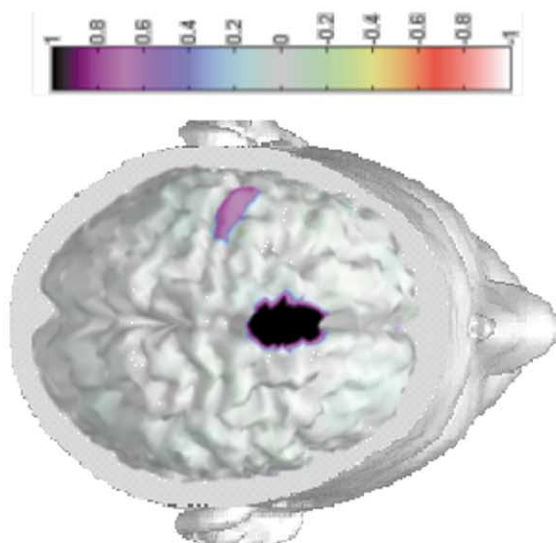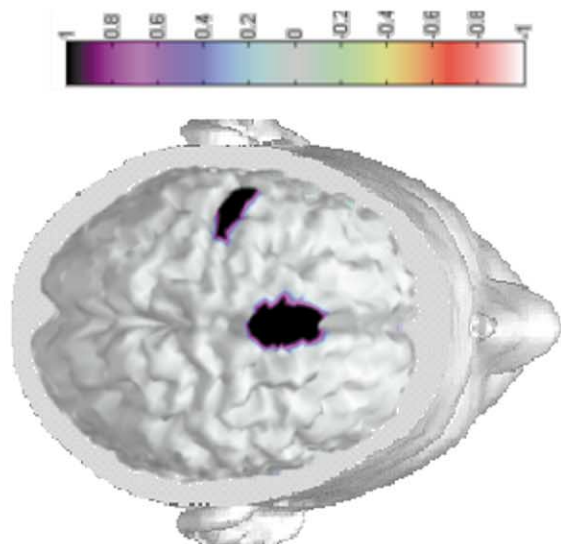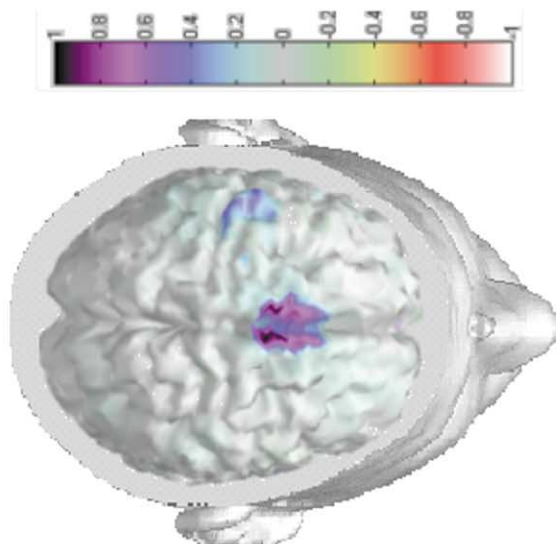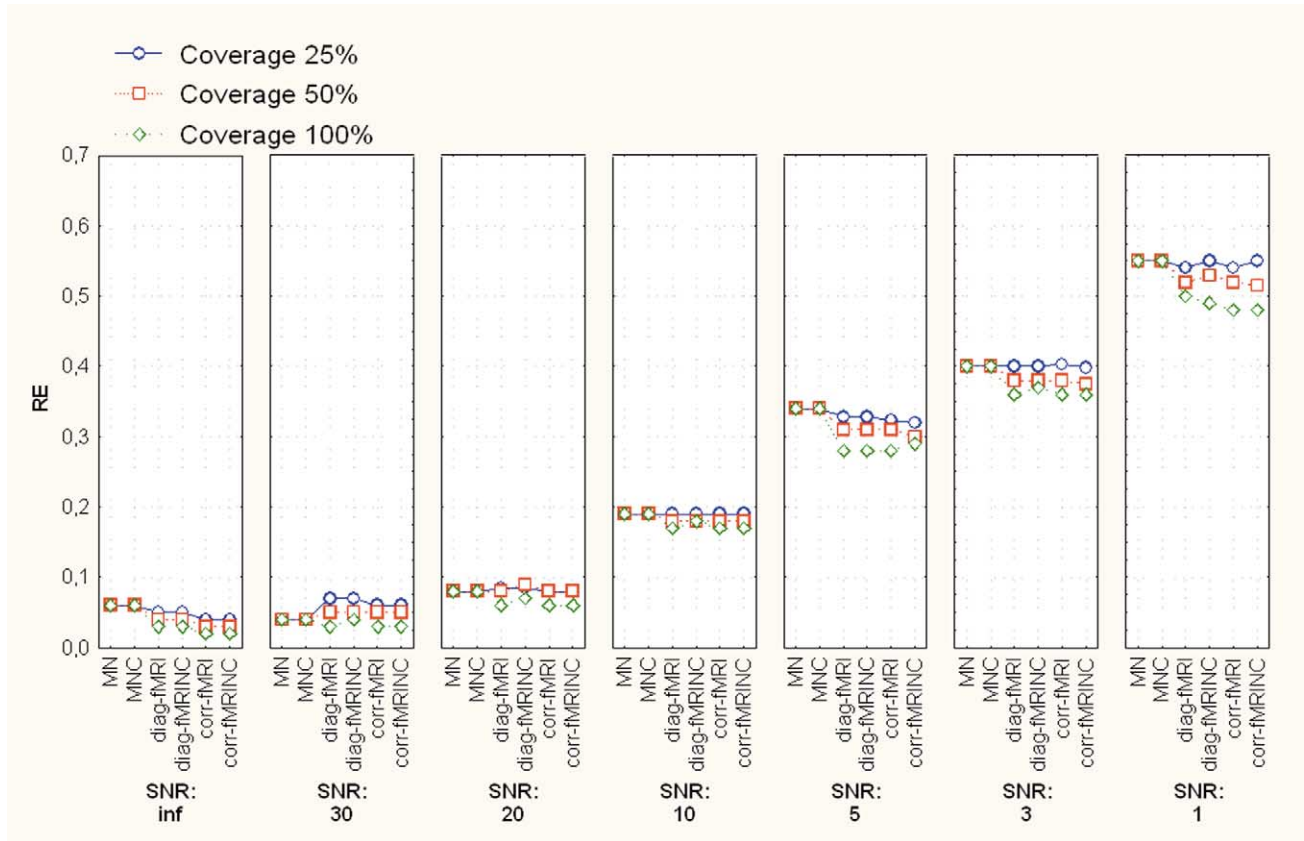
Fig. 6. Average data for relative error (RE) index in the ROI representing the SMA, at the different levels of the main factors considered (fMRICOVERAGE, INVERSE, and SNR). Simulations performed at 128 electrodes and with a level of fMRI strength of $K = 3$. Same conventions used as in the Fig. 3.

tors used here (MN, MNC). This occurs when the simulated EEG data showed a SNR variable from 10 to 1 (as stated by Scheffe's tests performed at $P < 0.05$). No statistical improvements in CC index were observed increasing the SNR of simulated EEG data from 20 to infinite and estimating cortical current density with the use of inverse methods with fMRI priors. No statistically significant difference in the CC index was reported among diag-fMRI- and corr-fMRI-based inverse operators under the whole range of the SNRs values used in the simulations. It was also observed that an increase of the number of simulated electrodes from 29 to 61 or 128 was useful to improve in a statistically significant way the estimation of the cortical activity (Scheffe's tests, $P < 0.01$).

A statistically significant decrease of values of RE by using fMRI-based inverse operators with respect to the other was obtained when the SNR of the simulated EEG data decreases from 5 to 1 (Scheffe's test, $P < 0.05$). In this context, statistically significant lower values of RE index were obtained for the corr-fMRI-based inverse operators with respect the diag-fMRI ones for a level of SNR = 1 (P

< 0.01), when 128 electrodes were used. However, such effect was absent for the other combinations of SNR values and number of electrodes investigated. In Fig. 3 are presented the average data of RE for the ROI representing the SMA, for the main factors analyzed (ELECTRODES, SNR and INVERSE). It is worth noting that the higher the SNR, the lower the RE index in the current density estimation for all the inverse operators and all the number of electrodes used.

ROIs without the presence of fMRI hotspots

Results are reported for the ROI right PP area to assure that the inclusion of the fMRI priors on left S1, left M1, and SMA did not simultaneously disturb the correct estimation of the cortical activity in the ROIs without fMRI hot spots (namely the right M1, right S1, and both the left and the right PP areas). The simulations were the same considered before for the ROIs with fMRI hot spots included. The three-way ANOVA was computed with the three main factors ELECTRODES, SNR, and INVERSE. The F values returned by the ANOVA for both the CC and the RE

Fig. 5. Current density estimates performed by the different inverse operators. The generated pattern is shown in the first top left map (Original). The estimates obtained with the MN, diag-fMRI, diag-fMRINC, corr-fMRI, and corr-fMRINC are presented in the successive maps. Estimations performed with 128 electrodes at SNR = 3. The level of fMRI strengths was set to 3 for the fMRI-based inverse operators.

indexes reported that only the main factors SNR and ELEC-TRODE significantly decrease the variances of the RE and CC indexes ($P < 0.0001$). The main factor INVERSE does not play a role in the improvement of the accuracy of the current density reconstruction in the ROIs without fMRI hot spots ($P < 0.18$; ns). A dependence of the CC and RE indexes for the variance reduction was observed on the number of ELECTRODES. In fact, the Scheffe's post hoc tests (performed at $P < 0.05$) report statistically significant differences between values of the RE and CC values when computed from 128 or 61 electrodes with respect to 29 electrodes. Instead, no relevant differences between the re-constructions of current density from 128 or 61 electrodes in the ROIs without fMRI hot spots were observed from analysis of post hoc tests. A slight influence of the SNR levels on the values of CC is visible in Fig. 4. A decrement of the correlation between the estimated and the generated wave-forms were observed by decreasing the SNR from infinite to 1 when 61 or 128 electrodes were used.

Fig. 5 shows the spatial distributions of the estimated current density strengths obtained by the different inverse methods with the fMRI coverage of 100% and the value of $K = 3$. In particular, the two instantaneous activated cortical areas were shown together with the reconstruction of the cortical current density performed with the MN, the diag-fMRI, the diag-fMRINC, the corr-fMRI, and the corr-fMRINC inverse operators. The reconstruction performed with the fMRI-based inverse operators attempt to recover the current density activation in both the two active cortical areas (namely the SMA and the left M1). The current density activity recovered by the conventional MN inverse operator suffered by a smoothness that makes it difficult to determine the cortical areas involved.

Evaluation of variable fMRI hot spot coverage at constant levels of the number of electrodes used (128) and strength of fMRI priors (k = 3)

ROIs with presence of fMRI hot spots

As described previously, the presented results are rela-tive to simulation setup in which the coverage of fMRI hot spots on the ROI analyzed was complete (100%). We also studied the effects of the variations of this independent variable, which is called fMRICOVERAGE. This was done by performing separate three-way ANOVAs for the CC and RE indexes under the condition of 128 electrodes used and fMRISTRENGTH at $K = 3$. Each ANOVA was performed by using the main factors fMRICOVERAGE (with three levels: 25, 50, 100%), INVERSE (six levels: MN, MNC, diag-MN, diag-MNC, corr-MN, and corr-MNC), and SNR (with seven levels: infinite, 30, 20, 10, 5, 3, and 1). At the $P < 0.0001$ level of significance, for the indexes CC and RE, statistically significant reductions of variances were obtained with all the main factors used and for their inter-actions.

In the case of the fMRI-based inverses, with SNR values

between 5 and 1, post hoc tests revealed that the quality of reconstruction was increased using a 100% percentage of fMRI coverage in the ROI analyzed compared to the use of 50 or 25%. Furthermore, with SNR values between 5 and 1, the quality of the estimation performed by fMRI-based inverse operator improved compared to the no-fMRI ones. This consideration holds for both the indexes used (CC and RE). For 25 or 50% the quality of the estimate at average or moderate SNR (20 to 1) is substantially equivalent to those returned by no-fMRI methods. In Fig. 6 are presented the average data of RE for the ROI representing the SMA, for the main factors analyzed (fMRICOVERAGE, SNR, and INVERSE). It is worth noting that the higher the fMRI-COVERAGE, the lower the RE index in the current density estimation for all the inverse methods used.

ROIs without the presence of fMRI hot spots

The effects of the variation of the fMRI hot spots per-centage coverage have been investigated also in the ROI without the presence of fMRI hot spots. The following shows the results for the right PP area. Equivalent results were found in all the ROIs investigated. The three-way ANOVA was performed for the right PP ROI with the main factors fMRICOVERAGE, INVERSE and SNR and with CC or RE as the dependent variable. A statistically signif-icant decrease in variance for CC and RE indexes was found only for the SNR main effect ($F(6,186)$) $= 22.1$; $P < 0,0001$). Hence, the effect of the increase of the percentage of fMRI coverage from 25 to 100% was not statistically relevant in cortical areas in which no-fMRI priors were used. A substantial equivalence of the effects of fMRI coverage was observed among the different inversion pro-cedures.

Discussion

The results of the present simulation study stated the general efficacy of the inverse operators used in the recov-ery of the generated cortical activity at the level of ROI. The recovery of the generated waveforms could be performed at different SNR levels and number of electrodes used. In particular, the indexes used stressed the capability of the inverse operators to estimate at least the 90% of the gener-ated waveforms, using a set of at least 61 scalp electrodes.

It may be argued whether the results presented here are valid only for the particular experimental task used to gen-erate the source waveforms used in simulations (right finger movements) or they can be generalized for any activation pattern among the selected ROIs. To address this problem we performed simulations with a different series of cortical generated waveforms, in which binary levels of activation in each ROI were illustrated. Any possible activation pattern for the analysed ROIs was considered. The results were absolutely consistent with those provided by the source reference waveforms used in the present study. The statis-

tical significance of the interactions among main factors in the different experimental conditions had the same level of significance of in the simulations presented here. This clearly indicates that the presented results were independent by the particular reference waveforms used.

As expected, there is a relevant effect of the noise levels on the estimation of current density. However, for any level of SNR, the higher the spatial sampling of the EEG distributions, the higher the quality obtained of the current reconstruction. Current density estimates improved significantly using 61 or 128 scalp electrodes instead of 29 electrodes. Comparing the use of both 128 electrodes and 61 electrodes for the different SNR levels, the 128 electrodes returned improved but not statistically significant values of CC and RE. Consequently, at least for the SNR normally encountered in literature (from 10 to 3), the estimation of cortical activity can be performed accurately by using realistic head and cortical models and recording the EEG with 61 electrodes.

The simulations results suggest that, under different experimental conditions, there is a substantial equivalence of the accuracy of current density estimation produced by inverse operators with and without column norm normalization (MN and MNC). However, it should be noted that the presented simulations were performed by constraining the neural sources to the cortical mantle. Column norm normalization has been introduced mainly for linear inverse systems dealing with a tomographic model of the brain, in which the cerebral source space for the solution was coincident with the whole head model (Pascual-Marqui, 1995; Grave de Peralta and Gonzalez Andino, 1998). It can be hypothesized that these results are due to the relative subtle differences in depth between the modeled sources in sulci and gyri of the built cortical surface and the electrodes scalp position.

For the inverse operators, the use of fMRI information in ROIs uniformly covered by fMRI hot spots (100% coverage) was compared to a scarce fMRI coverage (25%). A statistically significant improvement of the estimation of current density was observed in the case of 100% coverage. The 100% fMRI coverage of the ROI simulates ROIs located exactly at the fMRI hot spots. This procedure is often used in the recent published works on multimodal EEG/MEG and fMRI integration (Liu et al., 1998; Dale et al., 2000). The improvement in current estimates performed by corr-fMRI- and diag-fMRI-based inverse operators, compared to the MN and MNC inverse ones, is statistically significant in presence of moderate SNR values (5, 3, or 1). These SNR values are typically encountered in the analysis of EEG recordings obtained during motor and cognitive tasks. A substantial equivalence for all the inverse methods at high SNR values (from 20 to infinite) was observed when the percentage of the fMRI hot spots in the analyzed ROI moved down to 50 and 25%. The current density estimations performed by the fMRI-based inverse operators in ROIs without fMRI hot spots returned statistically similar performance indexes compared to the standard inverse methods (MN, MNC). Hence, fMRI-based inverse operators can be used to retrieve estimates of current density activity at the cortical level in ROIs with and without the presence of fMRI hot spots.

The results obtained by the application of the post hoc tests on the RE and CC indexes suggested that all the fMRI-based inverse operators here used return similar current density estimates under a large variety of SNRs levels and number of electrodes. However, for SNR = 1, the corr-fMRI inverse method, compared to the diag-fMRI methods, presented statistically significantly improved values of the RE and CC indexes. Simulations have been performed also by changing the tuning factor K for the fMRI-based inverse methods (diag-fMRI, corr-fMRI). The results stated that the optimal values for K are 3 and 10. Dale, Liu, and colleagues, by using the Bayesian formulation for the inclusion of the fMRI priors during MEG simulations, found that the optimal level of fMRI weighting for their inverse operator was of the order of 90% (Dale et al., 2000; Liu et al., 1998, 2002). It can be demonstrated that the Bayesian formulation of the fMRI-based inverse operators is closely equivalent to the deterministic one, presented here with the name of diag-fMRI. A formal proof of this equivalence can be found in Liu (2000). The optimal level of 90% for the fMRI weighting in the Bayesian formulation of Dale and colleagues was closely equivalent to the value of $K = 10$ for the diag-fMRI inverse operator here presented. Hence, there is a general level of agreement between the results here obtained for diag-fMRI inverse operators and those already presented for the multimodal integration of MEG and fMRI data (Liu et al., 1998; Liu, 2000; Dale et al., 2000). However, these results were increased in this article by taking into account several SNR levels, sensors numbers, and different computational schemes for fMRI priors.

Conclusions

There is a large consensus about the need and usefulness of the multimodal integration of metabolic, neurovascular, and electrophysiological data of neuronal activation. Results presented in the literature (reviewed in Dale and Halgren, 2001) and those presented here suggest that it is possible to improve the spatial details of the estimated neural sources by performing a multimodal integration of EEG and/or MEG with fMRI.

On the basis of the simulations performed we are able to answer to the questions posed in the Introduction:

1. There is a significant influence of the SNR and the number of electrodes on the estimation of cortical current density. This influence is similar because it uses a current estimation either with or without fMRI priors.

2. The use of fMRI priors increases the efficacy of the cortical current density estimation in the ROIs in which fMRI hot spots are present.
3. Simultaneously, the use of fMRI priors does not decrease the efficacy of the cortical current density estimation in the ROIs in which there are no fMRI hot spots.

In the multimodal integration of EEG and MEG data a precise electromagnetic theory and methodology exists (Baillet and Garnero, 1997; Baillet et al., 1999; Fuchs et al., 1998; Babiloni et al., 2001; Liu et al., 2002). However, it is still lacking a clear mathematical and physiologic link between metabolic demands and firing rates and characteristics (i.e., synchronicity, coherence) of the neurons (Nunez and Silberstein, 2000; also reviewed in Arthurs and Boniface, 2002). This physiological link is necessary since each neuroimaging technique (EEG, MEG, or fMRI) has its own visible and invisible sources. The visible sources for a particular neuroimaging technique are those neuronal pools whose spatiotemporal activity can be partly detected. In contrast, invisible sources are those neural assemblies that produce a pattern of the spatiotemporal activity not detectable by the analyzed neuroimaging technique. This can provide examples of neural activities that can be detected by fMRI measurements and not by EEG. For instance, because of their spatial arrangements, the stellate cells at the cortical level have a sustained metabolic demand (Braitenberg and Schuz, 1991) and they produced virtually no recordable electrical potential on the scalp surface. The opposite behavior can be found in cortical assemblies. They are active for a very short amount of time; therefore, they are insufficient to illustrate a detectable hemodynamic neurovascular coupling. However, the results presented here are referred to a more common situation in which neural sources are active for a sufficient period of time to illustrate a detectable hemodynamic signature. These results suggested that when using the fMRI priors the accuracy estimation of the cortical current density is increased.

References

Arthurs, O., Boniface, S., 2002. How well do we understand the neural origins of the fMRI BOLD signal? Trends Neurosci. 25, 27–31.

Babiloni, F., Babiloni, C., Carducci, F., Del Gratta, C., Romani, G.L., Rossini, P., Cincotti, F., 2002. Cortical source estimate of combined high resolution EEG and fMRI data related to voluntary movements. Methods Inform. Med. 41, 443–450.

Babiloni, F., Carducci, F., Cincotti, F., Del Gratta, C., Pizzella, V., Romani, G.L., Rossini, P.M., Tecchio, F., Babiloni, C., 2001. Linear inverse source estimate of combined EEG and MEG data related to voluntary movements. Hum. Brain Mapp. 14 (4), 197–210.

Baillet, S., Garnero, L., 1997. A bayesian framework to introducing anatomo-functional priors in the EEG/MEG inverse problem. IEEE Trans. Biomed. Eng. 44, 374–385.

Baillet, S., Garnero, L., Marin, G., Hugonin, P., 1999. Combined MEG and EEG source imaging by minimization of mutual information. IEEE Trans. Biomed. Eng. 46, 522–534.

Braitenberg, V., Schuz, A., 1991. Anatomy of the Cortex: Statistics and Geometry. Springer-Verlag, New York.

Cincotti, F., Babiloni, C., Carducci, F., De Gratta, C., Romani, G.L., Rossini, P.M., Angelone, L., Babiloni, F., 2001. The use of fMRI priors for the estimation of cortical activity with high resolution EEG. Electromagnetics 21, 579–592.

Dale, A., Liu, A., Fischl, B., Buckner, R., Belliveau, J.W., Lewine, J., Halgren, E., 2000. Dynamic statistical parametric mapping: combining fMRI and MEG for high-resolution imaging of cortical activity. Neuron 26, 55–67.

Dale, A.M., Halgren, E., 2001. Spatiotemporal mapping of brain activity by integration of multiple imaging modalities. Curr. Opin. Neurobiol. 11 (2), 202–208.

Dale, A.M., Sereno, M., 1993. Improved localization of cortical activity by combining EEG and MEG with MRI cortical surface reconstruction: a linear approach. J. Cogn. Neurosci. 5, 162–176.

Fuchs, M., Wagner, M., Wischmann, H.A., Kohler, T., Theissen, A., Drenckhahn, R., Buchner, H., 1998. Improving source reconstruction by combining bioelectrical and biomagnetic data. Electroencephagr. Clin. Neurophysiol. 107, 69–80.

George, J.S., Aine, C.J., Mosher, J.C., Schmidt, D.M., Ranken, D.M., Schlitt, H.A., Wood, C.C., Lewine, J.D., Sanders, J.A., Belliveau, J.W., 1995. Mapping function in the human brain with MEG, anatomical MRI and functional MRI. J. Clin. Neurophysiol. 12, 406–431.

Grav de Peralta Menendez, R., Gonzalez Andino, S.L., 1998. Distributed source models: standard solutions and new developments, in: Uhl, C. (Ed.), Analysis of Neurophysiological Brain Functioning, Springer Verlag, New York, pp. 176–201.

Grinvald, A., Lieke, E., Frostig, R.D., Gilbert, C.D., Wiesel, T.N., 1986. Functional architecture of cortex revealed by optical imaging of intrinsic signals. Nature 324 (6095), 361–364.

Hämäläinen, M., Ilmoniemi, R., 1984. Interpreting Measured Magnetic Field of the Brain: Estimates of the Current Distributions. Technical Report TKK-F-A559, Helsinki University of Technology.

Hansen, P.C., 1992a. Analysis of discrete ill-posed problems by means of the L-curve. SIAM Rev. 34, 561–580.

Hansen, P.C., 1992b. Numerical tools for the analysis and solution of Fredholm integral equations of the first kind. Inverse Problems 8, 849–872.

Kim, S., Ashe, J., Hendrich, K., Ellermann, J., Merkle, H., Ugurbil, K., Georgopulos, A., 1993. Functional magnetic resonance imaging of motor cortex: hemispheric asymmetry and handedness. Science 261, 615–617.

Liu, A.K., 2000. Spatiotemporal Brain Imaging, PhD dissertation. Massachusetts Institute of Technology, Cambridge, MA.

Liu, A.K., Belliveau, J.W., Dale, A.M., 1998. Spatiotemporal imaging of human brain activity using functional MRI constrained magnetoencephalography data: Monte Carlo simulations. Proc. Natl. Acad. Sci. 95 (15), 8945–8950.

Liu, A.K., Belliveau, J.W., Dale, A.M., 2002. Monte Carlo simulation studies of EEG and MEG localization accuracy. Hum. Brain Mapp. 16, 47–62.

Logothetis, N.K., Pauls, J., Augath, M., Trinath, T., Oeltermann, A., 2001. Neurophysiological investigation of the basis of the fMRI signal. Nature 412 (6843), 150–157.

Magistretti, P.J., Pellerin, L., Rothman, D.L., Shulman, R.G., 1999. Energy on demand. Science 283 (5401), 496–497.

Malonek, D., Grinvald, A., 1996. Interactions between electrical activity and cortical microcirculation revealed by imaging spectroscopy: implications for functional brain mapping. Science 272 (5261), 551–554.

Nunez, P., 1981. Electric Fields of the Brain. Oxford University Press, New York.

Nunez, P.L., 1995. Neocortical Dynamics and Human EEG Rhythms. Oxford University Press, New York.

Nunez, P.L., Silberstein, R., 2000. On the relationship of synaptic activity to macroscopic measurements: does co-registration of EEG with fMRI make sense? Brain Topogr 13 (2), 79–96.

Pascual-Marqui, R.D., 1995. Reply to comments by Hamalainen, Ilmoniemi and Nunez. ISBET Newslett. 6, 16–28.

Puce, A., Allison, T., Spencer, S.S., Spencer, D.D., McCarthy, G., 1997. Comparison of cortical activation evoked by faces measured by intracranial field potentials and functional MRI: two case studies. Hum. Brain Mapp. 5 (4), 298–305.

Regan, D., 1989. Human Brain Electrophysiology: Evoked Potentials and Evoked Magnetic Fields in Science and Medicine. Elsevier Press, New York.

Scherg, M., von Cramon, D., Elton, M., 1984. Brain-stem auditory-evoked potentials in post-comatose patients after severe closed head trauma. J. Neurol. 231 (1), 1–5.

Sharbrough, F., Chatrian, G.E., Lesse, R.P., Luders, H., Nuwer, M., Picton, T.W., 1991. American electroencephalographic society guidelines for standard electrode position nomenclature. J. Clin. Neurophysiol. 8 (2), 200–202.